NOTAS DE FÍSICA

VOLUME II

Nº 13

STUDIES ON THE NUCLEAR PHOTOEFFECT

M. D. DE SOUZA SANTOS, J. GOLDEMBERG, R. R. PIERONI, E. SILVA

OTTAVIA A. BORRELLO, SUZANNA S. VILLAÇA

AND

J. LEITE LOPES

CENTRO BRASILEIRO DE PESQUISAS FÍSICAS

Av. Wenceslau Braz 71

RIO DE JANEIRO

1955

STUDIES ON THE NUCLEAR PHOTOEFFECT*

M. D. de Souza Santos, J. Goldemberg, R. R. Pieroni, E. Silva
Ottavia A. Borrello, Suzanna S. Villaça

Laboratório de Física Nuclear, Universidade de São Paulo
São Paulo, S. P.

and

J. Leite Lopes

Faculdade Nacional de Filosofia, Universidade do Brasil, and
Centro Brasileiro de Pesquisas Físicas
Rio de Janeiro, D. F.

(November 1, 1955)

I. INTRODUCTION

In the experiments described in this paper, the source of X-ray of a variable energy was a 24 MeV Betatron of Kerst's design[1,2,3]. The magnet was made by Allis-Chalmers Mfg. Co. and the machine and auxiliary circuits were installed by the laboratory staff of the University of São Paulo.

---

* This paper was presented at the International Conference on the Peaceful Uses of Atomic Energy, United Nations, Genova, August 8 - 20, 1955.

Although the electronic circuitry is conventional in its main aspects and follows quite closely the University of Illnois design[2,3], some circuits, however, were developed at our laboratory in order to provide the machine with a long term stability of the electron beam energy.

Our machine has been in operation since 1951; the experience accumulated during the first years of operation has shown that most of the difficulties connected with the energy stability of the beam were due to the energy control system which was similar to the precision device used at the University of Saskatchewan[4].

Fundamentally, the energy control in an induction accelerator is obtained when the magnetic field, which determines the momentum of the electrons at the equilibrium orbit, reaches a pre-determined value. It is not easy, however, to measure directly this magnetic field so that use is made of a method developed at the University of Illinois[2,3].

Although the magnetic induction B, which determines the electron momentum is not easily obtained, the applied e.m.f. across the magnet coils is immediately available. This e.m.f. determines the rate of change of the guide field; its time integral represents, therefore, a measure of the magnetic induction B and, hence, of the momentum of the electrons at the equilibrium orbit. The voltage developed across the armatures of a condenser, charged by this e.m.f. through a large resistance, is a direct measure of the required instantaneous value of B and is available as a voltage of the same frequency of,

and practically in phase with, B, provided that the R/C ratio is properly chosen.

In our energy control circuits this integrated e.m.f. is compared with a pre-determined adjustable e.m.f. in a double triode amplitude comparison circuit whose characteristics can be checked at any time. Whenever the variable voltage just equals the reference e.m.f., a signal is delivered to the grid of the expander circuit and the beam is expanded on to the target. The circuits used for this purpose are illustrated in figures 1, 2, 3, 4 and 5.

Most of the work described in this paper was carried out with a pumped donut provided with a thin gold radiator which was attached to the injector structure and located at 1.2 cm. from the equilibrium orbit. Previous experiments[5] have shown that no multiple passages did occur under the experimental conditions used.

The machine was excited by means of an alternator driven at a pre-determined frequency by means of an electronically controlled magnetic clutch. This device allowed the machine to be driven at its resonant frequency under constant magnet excitation during the experiments: by this procedure, no frequency effects[6] on the energy scale were observed and the amplitude effects[6] was, under the most unfavourable conditions, smaller than 16.4 keV per a one volt change in magnet amplitude.

During a six month period, in which most of the experiments were made, it was found that the most common cause of drift in the energy control was due to a temperature effect in

the integrator resistance stuck. This is a systematic error which was eliminated by immersing the RC network in a temperature controlled oil bath. A smaller temperature systematic effect could still be observed and was duly corrected by keeping the Weston standard cell, used to check the reference voltage of the energy control circuit under constant temperature. With these precautions it was found that a very small effect (smaller than 1/5,000) could be attributed to a 40°C change in the magnet temperature. This systematic error, when required, can be corrected by measuring the magnet temperature at the different irradiations.

By using the procedure outlined above, it was possible to keep the energy stability of the machine within 3 keV (for an electron beam energy of 17.5 MeV) in short periods, whereas the long term stability is of the order of 10 keV. A typical stability curve, for which the above discussed temperature effects were not corrected, is reproduced in figure 6.

The measurement of the machine energy stability was made by means of repeated irradiations, at different times, of a boric acid pressed cylinder in a region of the activation curve of oxygen (15) for which the slope was 1.5% per a 10 keV change in energy.

II. THRESHOLD DETERMINATIONS

The excitation functions of photoinduced nuclear reactions show that as the peak energy of the Bremsstrahlung spectrum is increased, the cross-section for photodisintegration rises slow-

ly from zero at the threshold energy E_t and reaches a maximum in the region of the so-called giant resonance. Near the threshold, the behaviour of the excitation function depends on the disintegration process investigated, on the nature of the process responsible for the absorption of the bombarding photon and, in the particular case in which a single neutron is emitted, on the angular momentum of the outgoing particle.

At low energies (of the order of 10 MeV), magnetic dipole and electric quadrupole absorption are important and start to drop at about 20 MeV. At high energies, however, the absorption is strongly increased by the onset of dipole absorption[7].

The examination of the behaviour of the excitation function near the threshold has been discussed by several investigators[8,9,10] experimental data available show that although there are several instances in which the excitation function rises slowly due mainly to magnetic dipole and electric quadrupole absorption, there are several others for which a steep rise is observed and the cross-section analysis shows only the contribution due to the giant resonance (dipole absorption). A rapid rise in activity is thus expected whenever the energy of the incoming photons exceed the threshold energy.

In the instances however, where the threshold for the process under consideration is located in the region of magnetic dipole and electric quadrupole absorption, a slow increase of activity with the excess energy of the bombarding photon over the threshold is to be expected.

The considerations sketched above show that an accurate

experimental determination of the thresholds for photonuclear reactions can only be obtained through the extrapolation of an experimental curve whose shape cannot be predicted accurately (due, mainly, to the lack of precise knowledge of the shape of the tail of the Bremsstrahlung spectrum); as the obtained curves are smooth in a small region and since in most cases its curvature cannot be significantly appreciated, a good fit is obtained by calculating the least squares straight line and extrapolating it to zero yield.

Sometimes a parabolic rise is observed at the threshold; in this case a least squares fit of a quadratic expression is the best criterion available; a point is then determined unambiguously and is considered as a measurement of the threshold energy. A further check on this value can be obtained by observing the induced yield for energies just slightly below or above this extrapolated energy. In some instances, this has turned out to be quite an accurate procedure to locate a threshold within an error of 0.1%. This is a tedious procedure, however, since the activities are usually just above the natural background.

Another procedure which can be used to determine unambiguously the extrapolation point was suggested by Parsons And Collie (1950) and has been used widely by several investigators[11,12]. If one assumes that the yield Y for a given process increases with some power n of the photon excess energy over the threshold, $(\Omega - \Omega_0)$; a plot in a double logarithmical scale of the expression $Y = k(\Omega - \Omega_0)^n$ allows the value of the

threshold to be calculated . Since however, an assumption is made on the behaviour of the excitation function near the threshold, this value, although unambiguously determined, may be different from the actual threshold.

The measured thresholds reported in this paper were obtained by means of the induced activity technique and the least squares extrapolation, as described above, was used in most instances.

III. EXPERIMENTAL ARRANGEMENT

Cylindrical samples of compressed material under about 8,000 psi were used in most cases. They were designed to fit snugly over a Victoreen Thyrode counter encased in a lead castle. The thickness of the samples was chosen in every instance in order to get a source of infinite thickness. This procedure was chosen in order to get the maximum counting rate under a given irradiation.

The cylindrical samples were irradiated at 30 cm. from the X-ray target and the irradiation dose was measured by means of a Victoreen thimble ionisation chamber immersed in a lucite block whose sides were 3 cm. long[13]. Whenever high doses of irradiation were necessary, a Hanmer dosimeter was used under the same experimental conditions.

IV. ENERGY SCALE

The energy control system of the University of São Paulo's betatron gives a linear dependence between the variable referen-

ce e.m.f. and the momentum of the electrons at the equilibrium orbit prior to the expansion of the beam towards the X-ray target. This dependence can be verified at any moment during irradiation by means of the checking controls incorporated in the circuit. In particular, it is possible to calibrate the energy scale by means of a DC variable e.m.f. connected to the input of the cathode follower tube. This circumstance has turned out to be an useful feature to provide a quick check on the working conditions of the whole energy control system[6]. It can be shown that the relationship between the kinetic energy of the electrons that strike the target at a pre-determined value of the reference voltage energy control is given by

$$\left[E_{max}(E_{max} + 1.02) \right]^{1/2} = A (R + B) \qquad (1)$$

where R is the variable arm of the reference e.m.f. potentiometer and A and B constants. A depends upon the constants of the integrator and energy control circuits, the radius of the equilibrium orbit, the target radius, the true phase shift between the magnetic field and the integrated voltage across the condenser of the integrator stack and of the characteristics of the pulse applied to produce the expansion of the orbit towards the target[14].

These constants could be both, in principle, calculated without difficulty since B represents the displacement of the reference voltage introduced by the standing current in the cathode follower dropping resistance; this voltage can be accurately measured by means of either a sensitive voltmeter or by

a potentiometer.

The constants A and B were both determined experimentally by measuring the thresholds of (γ , n) reactions in light elements. Equation (1) was used then as an interpolation formula and it will be seen that the linear relationship holds within the accuracy of the experimental data. Indeed, since nuclear masses are not yet well enough known to enable small departures from the ideal conditions assumed in the derivation of this equation are thus found to be smaller than the errors introduced by mass-differences.

The thresholds used in this calibration were[15]

$$N^{14}(\gamma , n)N^{13}$$
$$O^{16}(\gamma , n)O^{15}$$
$$C^{12}(\gamma , n)C^{11}$$

which are, respectively, 10.545 ± 0.0163 MeV, 15.957 ± 0.012 MeV, and 18.707 ± 0.027 MeV. Those values should still be corrected by the energy of the recoiling nucleus after the photon capture

$$E_r = E_\gamma^2 / 2mc^2$$

and we get then 10.549 ± 0.017 MeV, 15.605 ± 0.012 MeV and 18.728 ± 0.027 MeV respectively.

Although the DC check on the energy scale calibration leads one to the certainty that there is a linear relationship between the reference voltage (as measured by the potentiometer arm R in ohms) and the momentum of the electrons at the equilibrium orbit, the introduction of a third point allows a better

interpolation of equation (1) in the experimental data.

V. EXPERIMENTAL RESULTS

1 - Nitrogen

Cylinders of dicyandiamide ($N_4C_2H_4$) compressed under 8,000 psi were used in these determinations. The samples used fit snugly over the thyrode counter used to detect the N^{13} activity induced by the (γ , n) process in N^{14}. The purity of the samples used was checked by measuring its decaying activity during several half-lives ($T_{1/2}$ = 10.1 min.).

The obtained activities as a function of the maximum energy of the betatron X-rays are illustrated in figure 7, where the points were obtained in integrator steps of 100 ohms. The extrapolated threshold occurs at 21,850 ohms. It can be observed that there is a sharp break at 23,200 ohms which corresponds to the contribution of an excitation level in the N^{14} excited nucleus and which had not been observed before by betatron irradiation. This level occurs at 11.38 MeV and has been observed by several investigators as quoted by Ajzenberg And Lauritsen[16].

2 - Oxygen

Samples of compressed boric acid, also under 8,000 psi were used in this experiment. A purity test was made by following the induced activity due to O^{15} during several half-lives. The excitation function obtained is illustrated in figure 8. There is also a sharp break of the excitation function which is attributed to an excitation level in the O^{16} nucleus and which

has been observed before[10,17]. The extrapolated threshold for this (γ , n) reaction occurs at 30,440 ohms.

3 - Carbon $C^{12}(\gamma , n)C^{11}$

In order to study the $C^{12}(\gamma , n)C^{11}$ reaction, pieces of polyethylene tubing were used. A check on their purity was made by irradiating the samples during one half hour and following the induced activity for several half-lives; a pure C^{11} activity of 20.5 min. half-life was observed.

The obtained extrapolated threshold lies at 35,600 ohms. The small activity, just above background was found to be a 10 minute half-life activity ascribed to the $N^{14}(\gamma , n)N^{13}$ reaction in N impurities, figure 9.

With the data obtained on these three reactions, a least squares fit was made to eq. (1) which can then be written as

$$\left[E_{max} (E_{max} + 1.02)\right]^{1/2} = - 2,428 + 0.593 R$$

This equation has been used in the determination of the thresholds of the reactions which will be described below.

4 - Chlorine: $Cl^{35}(\gamma , n)Cl^{34}$

The threshold for this reaction can be computed by taking into account the known mass differences of both nuclides [18]; since the maximum energy of the emitted positrons form Cl^{34} is known to be 4.5 MeV, the threshold for the process is found[19] to be 12.58 $\pm$ 0.09 MeV.

The threshold was determined by means of the induced

activity in a C Cl_4 samples measured in a liquid counter. A pure 33 minute ($T_{1/2}$) activity was observed and constitutes an inde - pendent check on the purity of the C Cl_4 employed in our measure ments. The obtained results are represented in figure 10. The ob served threshold for this reaction is found to be 12.55 ± 0.055 MeV.

5 - Iron: $Fe^{54}(\gamma , n)Fe^{53}$

Cylindrical samples of iron were used in this experiment and their purity was known by chemical analysis and was further checked by the induced activity under betatron irradiation. The threshold is located at 24,150 ohms which corresponds to 11.90 ± 0.07 MeV (Figure 11). The previous values for the thres- hold of this reaction were quoted as 14.2 ± 0.4 MeV[20] and 13.3 ± 0.2 MeV[6]. This value of the threshold corresponds to the rapid rise of the activity which is found in the region C of fi gure 11. One should expect this region to be the beginning of the contribution due to electric dipole absorption whereas the slow initial rise is a contribution of both magnetic dipole and electric quadrupole absorption. This region was missed by the investigators that examined this reaction before.

In order to examine whether this activity was not due to impurities, a very careful series of tests was made. The half-li fe of the induced activity in the region BC was measured in each point and was found to be typical of the Fe^{53} activity ($T_{1/2}$ = 9 min.). A chemical analysis of the samples showed no traces of copper in the amounts required to be responsible for the yields observed.

6 - Copper: $Cu^{63}(\gamma, n)Cu^{62}$

Electrolitic copper cylinders were used and their purity was examined by radiactive procedures. Special care must be exercised in this threshold determination owing to the fairly large capture cross-section of Cu^{65} for slow neutrons, leading to the 5 minute half-life activity of Cu^{66}.

The obtained results are illustrated in figure 12 where the extrapolated threshold occurs at 21,870 ohms which corresponds to 10.54 ± 0.04 MeV. This value agrees with Birnbaum's[12] observed threshold within the experimntal errors. Previous measurements have located this threshold at[20] 10.90 ± 0.2 and[3,21] 10.90 ± 0.2 and 10.8 ± 0.2.

Since it is usual to calibrate the betatron energy scale with the $Cu^{63}(\gamma, n)Cu^{62}$ threshold as a standard point, this error must have influenced a number of earlier threshold measurements.

The threshold value as calculated from mass differences gives[22] 10.00 ± 0.10. Since no cascade gamma-rays between 550 and 650 keV has been observed [25] the mass-difference must have an error of 540 keV.

7 - Zinc: $Zn^{64}(\gamma, n)Zn^{63}$

Cylinders of pure zinc were irradiated and the residual activity was measured in our standard arrangement for cylindrical samples. The obtained results are illustrated in figure 13. Below the threshold an activity of 5 minute half-life was detected and found to be due to $Zn^{67}(\gamma, n)Cu^{66}$. If the contribution

of this activity is subtracted, the extrapolation gives for the threshold 23,620 ohms which corresponds to 11.58 ± 0.06 MeV.

The same extrapolated value was obtained by extrapolating to zero yield by means of the procedure described by[9] Parsons and Collie as illustrated in figure 14. This value agrees within the experimental errors with the threshold as calculated by using mass differences[22] as 11.435 ± 0.053 MeV.

8 - Zirconium: $Zr^{90}(\gamma, n)Zr^{89}$

Discs of pressed zirconium oxide were irradiated at several betatron energies and the decay of the 4.4 minute activity was followed by an automatic counting system; the results are presented in figure 15 which locates the threshold for this reaction at 24,100 ohms, what corresponds to 12.20 ± 0.06 MeV. The values previously obtained for this threshold by other investigators were[24] 12.1 ± 0.1 and 12.3.

9 - Silver: $Ag^{109}(\gamma, n)Ag^{108}$

Silver cylinders were used as samples in these experiments and were irradiated at several betatron energies. Since Ag^{107} has a high cross-section for slow neutron capture, it is impossible to avoid some contribution of this process even for irradiation energies below the threshold and which is ascribed to neutrons originated both in the X-ray target and donut walls. By subtracting this contribution in the yield curve, the threshold can be located at 15,900 ohms which corresponds to 8,78 ± 0.04 MeV (figure 16). Previous values of this threshold were:[20;11;12] 9.3 ± 0.5; 9.05 ± 0.2; and 9.07 ± 0.7.

10 - Samarium: $Sm^{144}(\gamma, n)Sm^{143}$

Discs of pressed Sm_2O_3 were irradiated at different betatron energies and the induced 9.03 minute half-life activity measured in our standard counting arrangement. The obtained results located the threshold at 9.60 ± 0.05 MeV (figure 17).

CROSS-SECTIONS

In the course of the experiments carried out in our laboratory cross-sections for several photonuclear reactions were computed by means of the photon difference method[25].

In this paper, some typical or peculiar ones will be described.

1 - Chlorine: $Cl^{35}(\gamma, n)Cl^{34}$

2 - Potassium: $K^{39}(\gamma, n)K^{38}$

Cylinders of compressed KCl at a pressure of 8,500 psi were used in these experiments and irradiated by the betatron as shown in figure 18. The samples were irradiated for a period of time of the order of ten minutes and the decay of the induced activities was followed for three hours: the activities measured were the 33 minutes half-life positron emitter Cl^{34} and 7.7 minutes $(T_{1/2})K^{38}$. The dose to which the samples were submitted was measured by means of a Victoreen condenser r-meter.

Analysis of the decay curves obtained at several energies gave the initial saturated activity induced in the samples. The absolute rate of disintegration was determined by computing the

number of active nuclei in an irradiated disc of compressed KCl, since for discs the determination of the geometric efficiency of the counting arrangement is less cumbersome. Corrections were made for self-absorption and self-scattering.

The disintegration scheme used in these computations for Cl^{34} is that given by King[19] and for K^{38} the one quoted by Low and Townes.[26] The results obtained for the activation curves are represented in figure 19. From these one can obtain the cross-sections for the (γ , n) reactions in Cl^{35} and K^{39}. The results are shown in figure 20.

The significant data obtained form these curves is presented in the table below.

Element	Threshold	$\sigma(E_{max})$	E_{max}	$\int \sigma dE$ MeV · b	Width (MeV)
Cl^{35}	12.35	7.4 mb	13.75 MeV	0.02	3.3
K^{39}	13.00	13.0 mb	18.25 MeV	0.04	2.6

3 - Zinc: $Zn^{64}(\gamma , n)Zn^{63}$, $Zn^{64}(\gamma ,2n)Zn^{62}$ and $Zn^{66}(\gamma ,\overline{np})Cu^{64}$

Cylinders of pure zinc were irradiated at a distance of 30 cm. of the betatron target during times ranging from 5 to 20 min., and the activity induced was measured by a cylindrical counter for 72 hours; in this way it was possible to separate the activities originated in the following reactions:

$Zn^{64}(\gamma , n)Zn^{63}$ with a half-life of 38 minutes, emitting positrons of 2,36 and 1,40 MeV.

$Zn^{64}(\gamma , 2n)Zn^{62}$ of half-life of 9.3 hour, emitting positrons

of 0.66 MeV, in equilibrium with Cu^{62}.

$Zn^{66}(\gamma, {}^{d}_{np})Cu^{64}$ with half-life of 12.8 hours emitting positrons of 0.57 MeV and beta rays of 0.66 MeV.

The 9.3 and 12.8 hour activities were separated by absorption techniques. Some activity due to Zn^{68} formed by neutron capture in Zn^{67} with 14 hours of half-life had to be subtracted from the long lived isotopes mentioned above.

The absolute rate of disintegration of a Zn disc was determined by comparison with a Copper sample irradiated in the same conditions; the other activities were determined by comparison with the 38 minutes activity. It was possible in this way to obtain the activation curves for the reactions listed above; the results are shown in figures 21, 22 and 23. From those curves the cross-sections of figures 24 and 25 were obtained. The activation curve for the $Zn^{64}(\gamma, 2n)Zn^{62}$ reaction determines the threshold for this reaction at 20.35 ± 0.35 MeV.

The results for the $Zn^{66}(\gamma, {}^{d}_{np})Cu^{64}$ are very interesting although measurements were not made above 22 MeV; at 21 MeV the ratio of the (γ, n) to the $(\gamma, {}^{d}_{np})$ cross-sections is 1.6: the same ratio computed from the evaporation model gives[7] 6.10^{3}. The yields for those reactions at the same energy is 200; this constitutes a confirmation of the results obtained by Byerly And Stephens for the emission of photodeuterons from copper[27]. The need of a special mechanism to explain the emission of photo-deuterons is clearly necessary.

4 - Sulfur: $S^{32}(\gamma, {}^{d}_{np})P^{30}$

Pressed cylinders of sulfur powder were irradiated at dif-

ferent betatron energies in the same arrangement already described for zinc measurements. The residual nucleus P^{30} is a 2.5 minute (half-life) positron emitter.

The activities obtained were compared to the activity of a boric acid sample in order to obtain the absolute rate of disintegration. The known activation curve for the reaction $O^{16}(\gamma , n)O^{15}$ was used for that purpose. The resulting activation curves and cross-sections are shown in figure 26.

The results obtained in this measurement can be compared with those of Katz And Penfold[28] for the same reaction. The first interesting point to observe is that our samples were 10 times heavier than those of Katz And Penfold; one can then be fairly confident of the results obtained close to the threshold. As we can see, in figure 26, the activation curve rises slowly from the threshold of the (γ , d) reaction at 19 MeV up to 20.5 MeV where the (γ , np) reaction comes in, and then increases rapidly; this can be interpreted as the contribution of the (γ , np) process that adds to the (γ , d). At these energies the ratio of the cross-section for the reaction (γ , n) as measured by Haslam et al.[29] to the $\left(\gamma , \frac{d}{np}\right)$ is six. Using the evaporation model one gets for the same ratio $\sim$ 400. Here we have again, clearly stressed, the need of a special mechanism to explain the emission of photodeuterons by nuclei.

5 - Iron: $Fe^{54}(\gamma , n)Fe^{53}$

Iron cylinders were used in a measurement of the activation curve of the (γ , n) reaction of the 9% abundant Fe^{54}. Special care was taken in the measurements of the energy region

immediately above the threshold, since this region presents some peculiarities.

The activation curve obtained in the form of counts per roentgen is shown in figure 27. The cross-section computed from it is shown in figure 28 normalized to the cross-section for the same process as measured at the University of Saskatchewan[25,28,30]. The agreement between the two curves is very good in the region of the dipole resonance, but, at lower energies our curve shows a knee typical of the contribution of magnetic dipole or lectric quadrupole absorption. This behaviour has been found before in light nuclei, like oxygen and nitrogen [31,32]. It is interesting to find this peculiarity in such a middle A nucleus like iron (A = 54) [33].

6 - Germanium: $Ge^{70}(\gamma, n)Ge^{69}$ and $Ge^{76}(\gamma, n)Ge^{75}$

Irradiation of natural germanium in the betatron beam allows the study of the following (γ , n) reactions:
$Ge^{70}(\gamma, n)Ge^{69}$ which decays into Ge^{69} by positron emission with a half-life of 40 hours, and
$Ge^{76}(\gamma, n)Ge^{75}$ which decays by beta ray emission into As^{75} with a half-life of 82 minutes.

A very small contribution to the activity is due to neutron capture reactions, but an analysis of the decay curves of irradiated Germanium permits the separation of the activities of Ge^{69} and Ge^{75}.

Samples of two grams of germanium were irradiated during ten minutes close to the betatron X-ray target and their activity was measured with an end window counter. In order to obtain

the absolute rate of disintegration the usual corrections were applied and the disintegration schemes quoted by King[19] were utilized.

The activation curves so obtained are shown in figure 29 and the corresponding cross-sections are illustrated in figure 30. The yields obtained at 18 MeV for the above reactions fit quite well the yield data of Price And Kerst[34]. The threshold obtained in our measurement for Ge^{70} at 12.1 ± 0.2 MeV indicates that the disintegration scheme for germanium 69 suggested by Way And Wood[35] is correct.

The cross-sections present the peculiarity of a maximum cross-section at an energy anomalously high; however as the obtained data were limited to a maximum energy of 22 MeV, it was not possible to obtain the falling part of the giant resonance. The shoulder present in the part of the cross-section immediately above the threshold indicates the presence of absorption of photons due to magnetic dipole or/and electric quadrupole.

The characteristics of the determined cross-sections are shown below

Element	Threshold	E_{max}	$\sigma(E_{max})$	$\int \sigma dE$
Ge^{70}	12.1 MeV	20 MeV	0.125 b	0.59 MeV - b
Ge^{76}	9.3 MeV	18.9 MeV	0.243 b	1.5 MeV - b

7 - Samarium: $Sm^{144}(\gamma, n)Sm^{143}$

Discs of pressed samarium oxide were irradiated at several energies in order to obtain the activation curve and cross-section for this reaction. Some effort was spent to obtain also more

information on the characteristics of the radioactivity induced in Sn^{144} by betatron irradiation.

The irradiated samples were counted with an end window counter and the decay curve followed for approximately 3 hours; besides a long lived activity present in the samples with a half-life of the order of 50 hours, an activity of the order of 10 min. half-life was observed. This activity has been found before by Butement[36] and assigned tentatively to Sn^{143}. As it will be shown this assignement is confirmed by our measurements.

The half life of this activity was accurately measured to be 9.03 ± 0.02 min. The disintegration scheme was studied roughly by absorption methods and the information was obtained that Sn^{143} decays by the emission of 2.6 MeV positrons; no other gamma-rays were found besides the annihilation radiation. Using this data, the activities obtained at a number of energies were compared with a copper sample irradiated in the same conditions, and the absolute rate of disintegration computed.

The activation curves so obtained are shown in figure 31; from this curve the cross-section was obtained and is shown in figure 32. The yield per mole/r/min at 18 MeV is $0.24.10^7$. Interpolating in the yield data of Price And Kerst[34] one gets for the same nucleus $0.93.10^7$; our result is then lower than the expected by a factor 4. If the reaction responsible for the 9.03 min. activity is Sn^{147}, which is the other possible assignement for this activity, our yield would be lower, by a factor of 20, than Price And Kerst's; this seems very unlikely to be the case.

The remaining disagreement of a factor 4 might be explained

by the existence of an undetected isomeric transition state in Sn^{143}; Sn^{143} belongs to one of the islands of isomerism indicated by Goldhaber And Hill[37] .

8 - Lead: $Pb^{207+208}(\gamma, p)Tl^{206+207}$

This reaction was studied in order to gain information on the validity of the evaporation model for the lead nucleus. Since the gamma-n cross-section has been measured before[38] the knowledge of the gamma-p reaction in the above mentioned isotopes might permit a comparison with theory.

The experiment can be made easily by residual activity methods since both Tl^{206} and Tl^{207} decay by emission of beta rays of approximately the same energy, 1.51 and 1.45 MeV respectively; besides that, the half-lives of these isotopes are approximately the same, 4.23 and 4.76 min.. Although a separation of the contributions from Tl^{206} and Tl^{207} was attempted using the fact that the first does not emit gamma rays whilst Tl^{207} emits some of 0.87 MeV, this attempt failled: a gamma-ray crystal spectrometer using a one-inch thick NaI scintillator was assembled but the relative intensity of the gamma-rays in Tl^{207} is so small[39] (0.005) that an insignificant number of counts were obtained.

The results of this work refer then to the sum of the contributions of Pb^{207} and Pb^{208}. Cylinders of natural lead were irradiated at several energies and counted in a cylindrical counter. Due to the high mass of the cylinders, it was possible to measure the activation curve down to 11 MeV; the thresholds for the reactions lie around 8 MeV[40].

The absolute rate of disintegration was determined irradi-

ating discs of Pb and Cu together and comparing their activities. After the usual corrections, the activation curve was obtained and is shown in figure 33; the cross-section computed from it, is shown in figure 34.

Using this cross-section and assuming that the gamma-n cross-section for the sum of the isotopes Pb^{207} and Pb^{208} is the same as the gamma-n cross-section for natural lead, one can compute at each energy the ratio $\frac{\sigma(\gamma, n)}{\sigma(\gamma, p)}$. The same ratio was computed from the evaporation model and the results are shown in the table below and in figure 35.

E(MeV)	Experiment	Evaporation model
12	135,000	-
13	13,000	-
14	7,400	$200{,}000 \times 10^4$
15	3,350	$17{,}000 \times 10^4$
16	1,470	$3{,}000 \times 10^4$
17	600	740×10^4
18	230	290×10^4
19	80	96×10^4
20	26	38×10^4

An analysis of this ratio shows that not only the evaporation model fails to account for the number of emitted protons by a factor 10^4 but, besides, it gets increasingly worse at low energies.

GENERAL DISCUSSION

The advent of the 24 MeV betatron has made it possible, in-

the last few years, to accumulate a wealth of information on the photonuclear processes in the intermediate energy range. It has turned out that, in most nuclides for which the different modes of decay of the compound nucleus has been examined, a valuable information on the behaviour of the processes responsible for the absorption of the electromagnetic radiation is obtained. In two particular instances in which the de-excitation of the compound nucleus by gamma-ray re-emission was studied, it has turned out that this effect is not larger than about 10% of the gamma-neutron mode of de-excitation[41,42]. On the other hand, it has been fairly well established that the de-excitation by a single neutron emission is the predominant mode of decay of the compound nucleus.

From the considerations outlined above it follows that a good estimate of the absorption processes of the electromagnetic radiation by the atomic nuclei is given by the analysis of gamma-neutron processes.

A common feature of the measured cross-sections for photonuclear reactions is that the cross-section rises slowly at threshold and stays practically constant for a while rising then in a typical bell-shaped curve which is often referred to as the giant resonance.

Several theories have been put forward to explain the nature of this giant resonance[43,44,45]; amongst these theories Levinger And Bethe's is based on considerations which are quite independent of the nuclear model. In particular, the integrated cross-section for photon absorption, as calculated by these

authors, make use of the quantum mechanical sum rules, and gives predictions which are well verified by the experimental dat available[46,38].

Another result of this theory is that the harmonic mean energy W_H for photon absorption, in the region of the giant resonance, can be expressed as a function of the mean squared displacement $\langle r^2 \rangle_{oo}$ of a nucleon, in the nuclear ground state, as

$$W_H = \frac{\int \sigma(E)\,dE}{\int \sigma(E)\,dE/E} = \frac{3\hbar^2}{2M} \frac{1 + .8x}{\langle r^2 \rangle_{oo}}$$

Here, $\sigma(E)$ is the nuclear absorption cross-section of photons of energy E, x is the fraction of the neutron-proton force which is of exchange nature and M is the nucleon mass.

As the integrals that occur in the equation above can be obtained from the experimental data, it is possible to compute $\langle r^2 \rangle_{oo}$ and, therefore, to gain some insight on the sub-units which are responsible, in a nucleus, for the dipole absorption.

In figure 36 is illustrated the behaviour of $\langle r^2 \rangle_{oo}$ as a function of A for the experimental data available and from the measurements reported in this paper. In the same figure two theoretical curves are drawn, corresponding to a model in which the neutrons are free to move inside the nuclear boundary, as defined by its radius, and for a model in which the sub-units responsible for photon absorption are assumed to be alpha-particles.

It seems that the available data strongly substanciates the model in which, most of the time, the nucleons are clustered

as alpha-particles.

An effect of closed shells on the photonuclear phenomena has been pointed out by Nathans And Halpern[47]; these investigators have found that magic nuclei show an anomalously narrow giant resonance half-width. The criterion used to evaluate the half-width, however, is not free from criticism since they consider in their measurements of the total neutron yield all the modes of de-excitation of the compound nucleus in which neutrons are emitted. As the thresholds for these processes are quite independent of the dipole absorption mechanism, fortuitous contributions may mask any effect that might be due to the shell structure. As, on the other hand, it is well established that the sudden rise of the cross-section of the giant resonance up to σ_{max} is in an interval of excitation for which the predominant mode of decay is by single neutron emission, a good criterion to avoid the difficulties just discussed could be to take into account the first half of the giant resonance curve to examine whether a magic number effect exists.

As one can see by examining figure 37, a good criterion to evaluate the onset of the dipole absorption for a given nucleus is to determine the point in which a straight line drawn through the points for which $\sigma_{1/2max}$ and σ_{max} intercepts the energy axis. The distances from this point to the energy at which σ is maximum is practically twice as large as one half of the half-width.

The results obtained by plotting δE against the atomic number are given in figure 38. The data used in these computations is given in the reference at the end of this paper. As one can

observe, there is no clear evidence for a magic number effect in this graph.

From very general considerations on the properties of magic number nuclides, one should expect that neutrons in an excited compound nucleus should have a smaller chance of being emitted as compared with a non-magic one at the same excitation energy. Indeed, as follows from Bohr's concept of the compound nucleus[48] the level density in a heavy nucleus increases rapidly with the excitation energy; it is obvious, therefore, that the sudden drop in the neutron binding energy which is observed in nuclei beyond magic numbers cause a corresponding increase of level density for the same excitation energy. This argument suggests a criterion to put in evidence any effect that might be due to shell-effects.

If we consider a typical cross-section as represented in figure 37, one can define a parameter Δ which is a magnitude dependent on the level density, and, therefore, takes into account the steepness of rise of the cross-section[48].

For magic nuclei and neighbours one should expect Δ to be larger than for the others. The results obtained by computing this parameter for several nuclides are represented in figure 39 and in Table I, for which the references are given below.

The shell structure is clearly exhibited in this curve at nuclides for which N is equal to 20, 28, 50, 82, 126 and the effect is greater for high mass-numbers.

The work described in this paper was supported with funds from the University of São Paulo, and, in part, by Conselho Nacional de Pesquisas.

TABLE I

Element	Z	N	A	Threshold		(MeV)	Reference
C	6	6	12	18.70	20.6	1.9	38, 49
N	7	7	14	10.54	19.3	8.8	51
O	8	8	16	15.60	21.8	6.2	51
Na	11	12	23	12.10	15.4	3.3	38
Mg	12	12	24	16.0	18.2	2.2	57
Al	13	14	27	14.0	17.5	3.5	38
Si	14	14	28	16.9	18.8	1.9	46
P	15	16	31	12.4	16.2	3.8	28
S	16	16	32	15.0	18.0	3.0	57
Cl	17	18	35	13.0	16.8	3.8	60
A	18	20	38	10.5	15.0	4.5	56
K	19	20	39	12.5	17.5	5.0	60
Ca	20	20	40	15.8	18.0	2.2	50
Cr	24	26	50	13.4	16.8	3.4	46
V	23	28	51	10.8	15.5	4.7	46
Mn	25	30	55	10.0	14.5	4.5	38
Fe	26	28	54	11.7	17.7	6.0	59
Co	27	32	59	10.2	15.0	4.8	38
Ni	28	30	58	12.0	15.5	3.5	30
Cu	29	34	63	10.6	14.5	3.9	52
Cu	29	36	65	10.2	14.1	3.9	52
Zn	30	34	64	11.6	14.5	2.9	58
As	33	42	75	10.1	13.0	2.9	38
Br	35	46	81	10.0	14.0	4.0	53
Rb	37	50	87	9.3	14.7	5.4	54
Nb	41	52	93	8.7	14.5	5.8	38
Mo	42	50	92	13.1	15.1	2.1	54
Ag	47	62	109	9.3	13.2	3.9	55
In	49	66	115	9.0	12.5	3.5	38
Sb	51	70	121	9.3	12.4	3.1	52
I	53	74	127	9.1	13.2	4.1	38
La	57	82	139	8.0	12.5	4.5	46
Pa	73	108	181	8.8	11.5	2.7	52
Au	79	118	197	7.3	11.4	4.1	38
Bi	83	126	209	7.4	11.6	4.2	38
U	92	146	238	6.0	9.5	3.5	56

1. Kerst, D. W., Phys. Rev., 58, 841 (1940)

2. Kerst, D. W., Phys. Rev., 59, 110 (1941a)

3. Kerst, D. W., Phys. Rev., 60, 47 (1941b)

4. Katz, L., McNamara, A. G., Forsyth, P. A., Haslam, R. N. H., and Johns, H. R. Can. J. Res. A 28, 113 (1950)

5. Goldemberg, J., Pieroni, R. R., Santos, M. D. S., and Silva, E., New Research Techniques in Physics. A Simposium, Acad. Bras. Ci. (1952)

6. Pieroni, R. R., Ph. D. Thesis (University of São Paulo) (1955)

7. Blatt, J. M. and Weisskopf, V. F. Theoretical Nuclear Physics. John Wiley and Sons, New York (1952)

8. Mc Elhinney, J., Hanson, A. O., Becker, R. A., Duffield, R. G. and Diven, B. C., Phys. Rev. 75, 542 (1949)

9. Parsons, R. W., and Collie, C. H., Proc. Phys. Soc. A 43, 859 (1950)

10. Collie, C. H., Santos, M. D. S., Pieroni, R. R., Silva, E. and Borello, O. Proc. of the 1954 Glasgow Conference on Nuclear and Meson Physics. Pergamon Press Ltd., London (1954)

11. Shorr, R., Halpern, J. and Stephens, W. E., Phys. Rev., 81, 154 (1951)

12. Birnbaum, M., Phys. Rev., 93, 146 (1954)

13. Johns, H. E., Katz, L., Douglas, R. A. and Haslam, R. N. H., Phys. Rev. 80, 1062 (1950)

14. Santos, M. D. S., Energy Control for Magnetic Induction Accelerators, Thesis, (University of São Paulo) (1953)

15. Li, C. H., Wahling, W., Fowler, W. A. and Lauritsen, C. C., Phys. Rev., 83, 512 (1951)

16. Ajzenberg, F. and Lauritsen, T., Rev. Mod. Phys., 24, 321 (1952)

17. Spicer, D. M., Penfold, A. S. and Goldemberg, J., Phys. Rev., 95, 629 (1954)

18. Segrè, E., Experimental Nuclear Physics. Vol. 1, John Wiley and Sons (1953)

19. King, A. A., Rev. Mod. Phys. 26, 327 (1954)

20. Baldwin, G. C., and Koch, H. W., Phys. Rev., 67, 1 (1945)

21. Mc Elhinney, J., and Ogle, W. E., Phys. Rev., 78, 63 (1950)

22. Duckworth, H. E. and Hogg, B. C., Can. J. Phys., 58, 258 (1953)

23. Hasbeun, R. L. et al., Physica XX, 8, 571 (1954)

24.Ogle, W. E., Brown, L. J., and Carson, A. H., Phys. Rev., 78, 63 (1950)

25.Katz, L. and Cameron, A. G. W., Can. J. Phys., 29, 518 (1951)

26.Low, W. and Townes, C. H., Phys. Rev., 80, 608 (1950)

27.Byerly, P. R. and Stephens, W. E., Phys. Rev., 83, 54 (1951)

28.Katz, L. And Penfold, A. S., Phys. Rev., 81, 815 (1951)

29.Haslam, R. N. H., Summers-Gill, R. G. And Crosby, E. H., Can. J. Rev., 30, 257 (1952)

30.Katz, L., Johns, H. E., Baker, R. G., Haslam, R. N. H. and Douglas, R. A., Phys. Rev., 82, 271 (1951)

31.Horsley, J., Haslam, R. N. H., and Johns, H. E., Can. J. Phys. 30, 159 (1952)

32.Johns, H.E., Horley, J., Haslam, R. N. H., and Quinton, A., Phys. Rev. 84, 856 (1951)

33.Professor L. Katz (University of Saskatchewan) remeasured recently the activation curve for this reaction, near threshold and found results similar to ours; he attributes however the anomaly found to a copper impurity (private communication). Although great care was taken in our measurement to avoid impurities, this point is being reinvestigated. (note added in proof correction.

34.Price, G. and Kerst, D. W., Phys. Rev., 77, 806 (1950)

35.Way, K. and Wood, M., Phys. Rev., 94, 119 (1954)

36.Butement, F. D. S., Proc. Phys. Soc., A64, 595 (1951)

37.Goldhaber, M. and Hill, R. D., Rev. Mod. Phys., 24, 179 (1952)

38.Montalbetti, R., Katz, L. and Goldenberg, J., Phys. Rev., 91, 659 (1953)

39.Suruguo, J., Comp. Rod., 212, 857 (1941)

40.Cameron, A. G. W., Burns, W. and Katz, L., Phys. Rev., 85, 1064 (1951)

41.Goldenberg, J. and Katz, L., Phys. Rev., 90, 308 (1953)

42.Del Rio, C. S. and Telegdi, V. L., Phys. Rev., 90, 489 (1953)

43.Goldhaber, M. and Teller, E., Phys. Rev., 74, 1046 (1948)

44.Levinger, J. S. and Bethe, H. A., Phys. Rev., 78, 115 (1950)

45.Levinger, J. S. and Rose, D. C., Phys. Rev., 95, 413 (1954)

46.Goldenberg, J. and Katz, L., Can. J. Phys. 32, 49 (1954)

47.Mathews, R. and Halpern, J., Phys. Rev., 93, 437 (1954)

49.Goldemberg, J. and Leite Lopes, J., Phys. Rev., 99, 1055 (1955)

50.Heslop, R. M. H., Johns, H. E., and Horsley, R. J., Phys. Rev. 82, 270 (1951)

51.Summers-Gill, R. G., Heslop, R. M. H., and Katz, L., Can. J. Phys. 31, 70 (1953)

52.Johns, H. E., Horsley, R. J., Heslop, R. M. H., and Quiton, R., Phys. Rev., 82, 856 (1951)

53.Johns, H. E., Katz, L., Douglas, R. A. and Heslop, R. M. H., Phys. Rev., 80, 1026 (1950)

54.Katz, L., Pearse, L., and Moody, H., Can. J. Phys., 30, 476 (1952)

55.Katz, L., Baker, R. G. and Montalbotti, R., Can. 31, 250 (1953)

56.Diven, B. C., and Almy, G. M., Phys. Rev., 80, 407 (1950)

57.Mc Pherson, D., Pederson, P. and Katz, L., Can. J. Phys., 32, 593 (1954)

58.Katz, L. and Cameron, A. G. W., Phys. Rev., 84, 1115 (1951)

59.This paper

60.This paper

61.This paper

62.Axel, P. and Fox, J. D., Phys. Rev., 95, 613 (A) (1954)

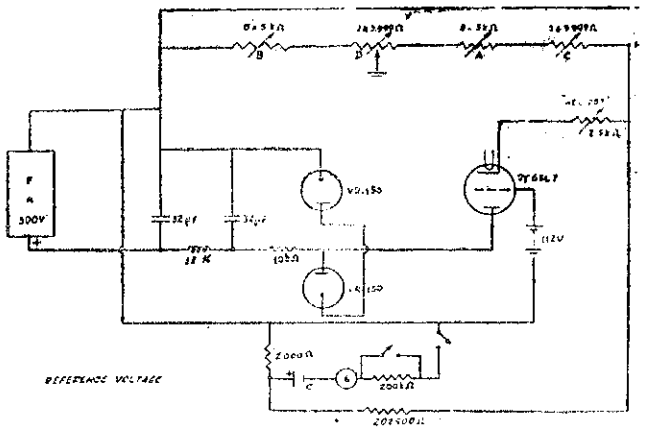

FIG. 1

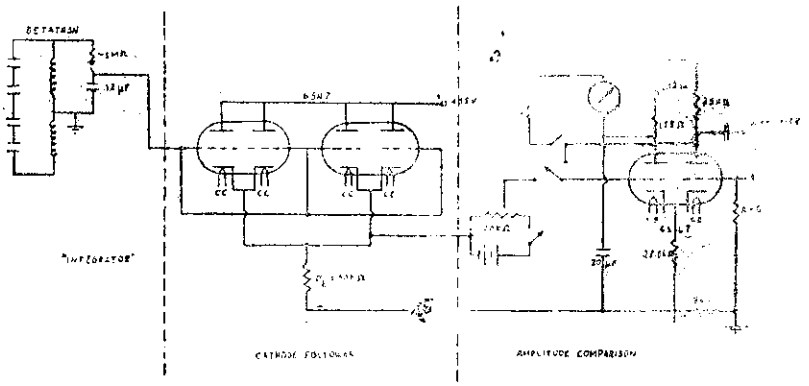

FIG. 2

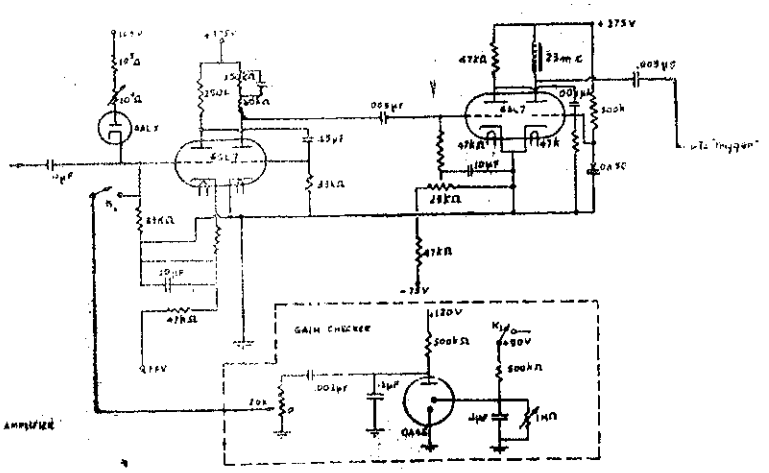

FIG. 3

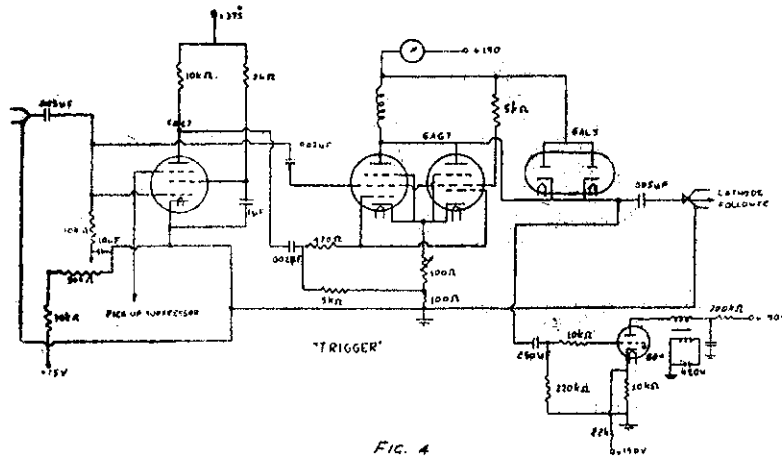
"TRIGGER"

FIG. 4

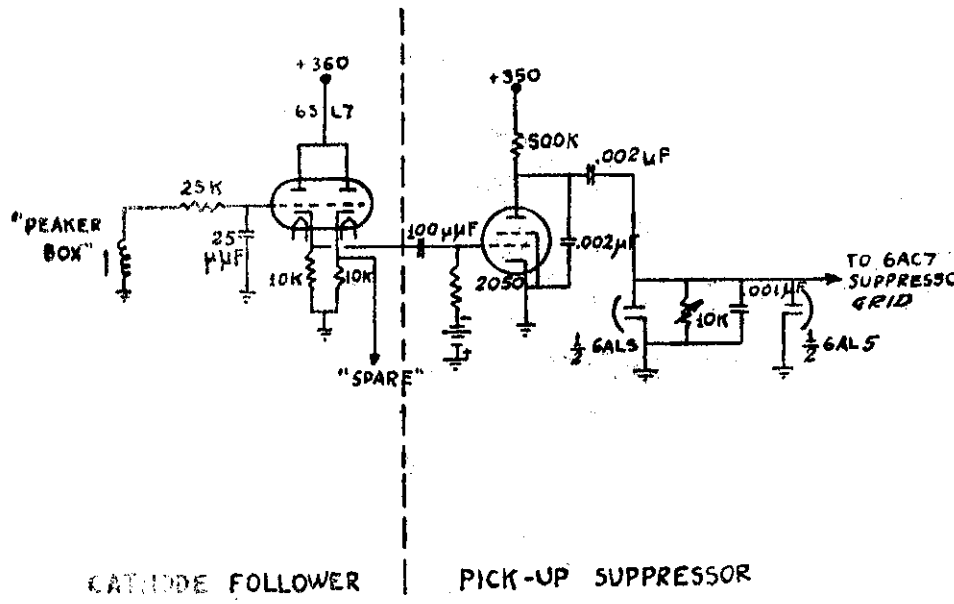
+360
6SL7
25K
"PEAKER BOX"
25 μμF
10K
10K
"SPARE"
100 μμF
+350
500K
.002 μF
.002 μF
2050
TO 6AC7 SUPPRESSOR GRID
.001 μF
10K
½ 6AL5
½ 6AL5
CATHODE FOLLOWER
PICK-UP SUPPRESSOR

Fig. 5

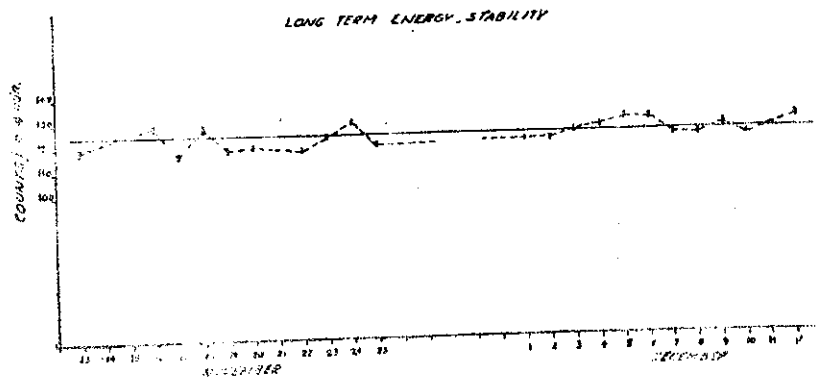
LONG TERM ENERGY STABILITY

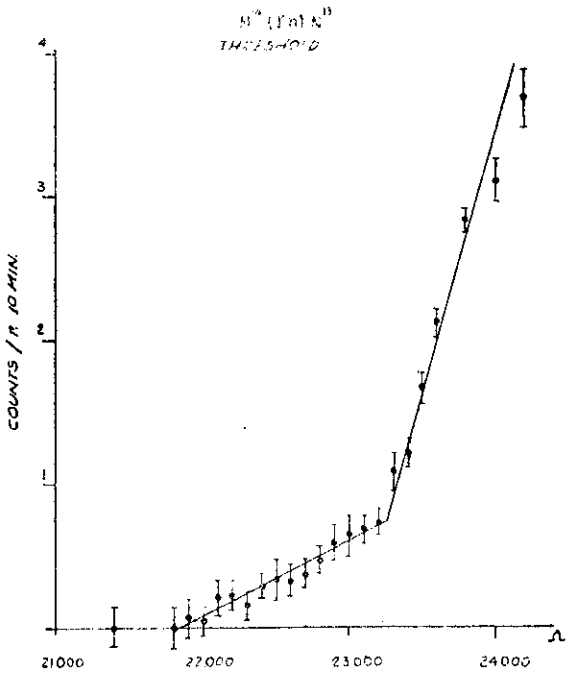

FIG. 7

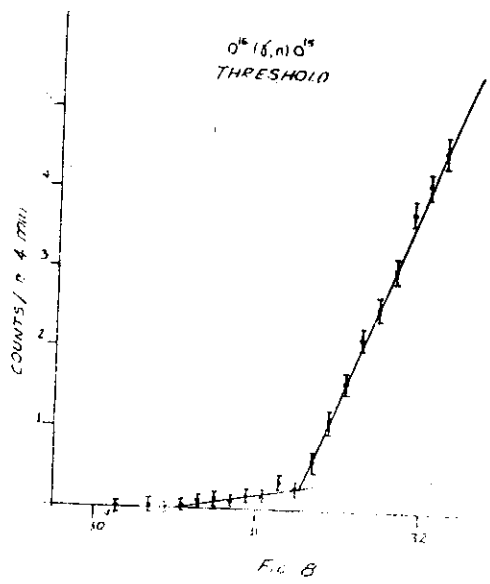

FIG. 8

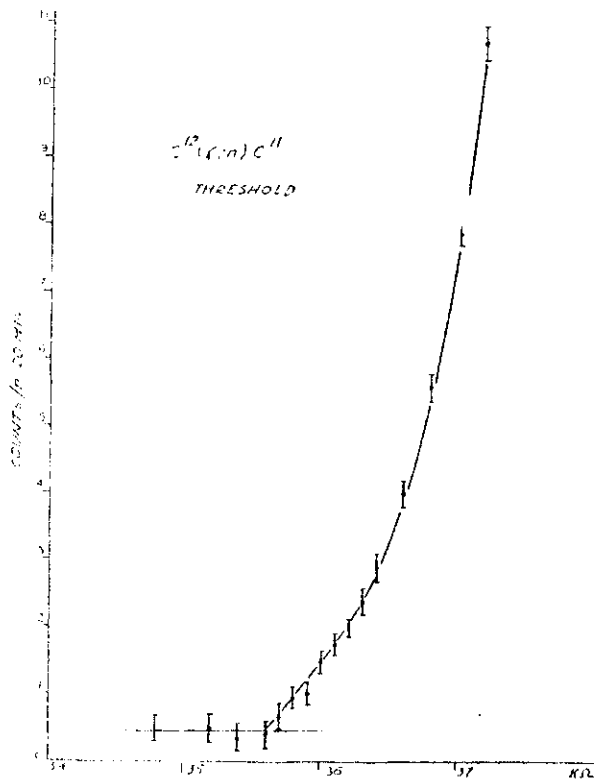

FIG. 9

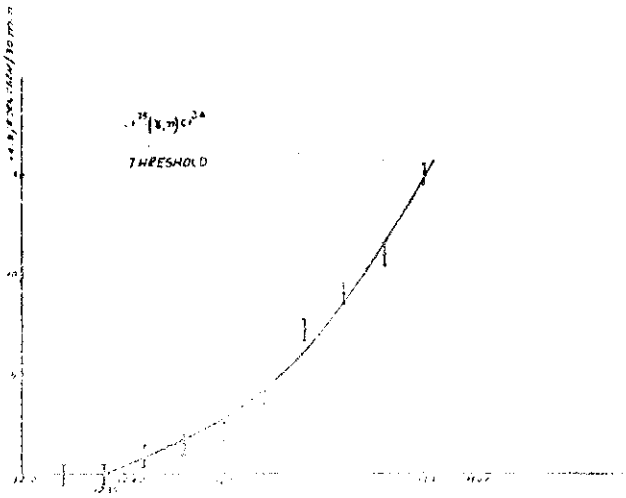

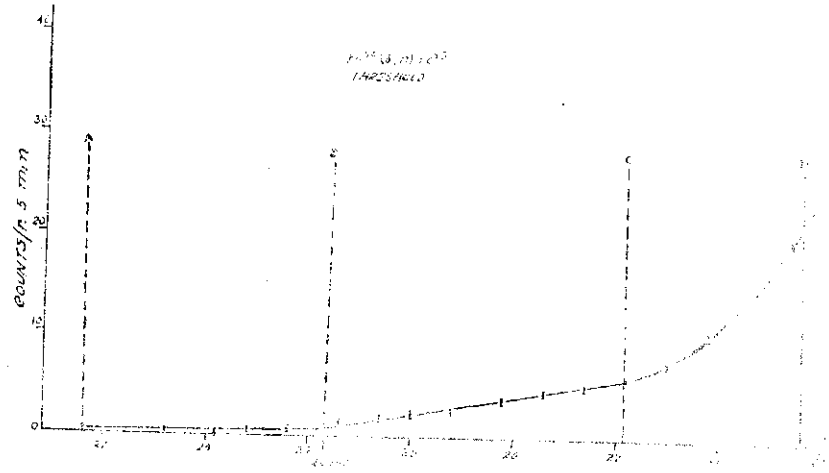

FIG.

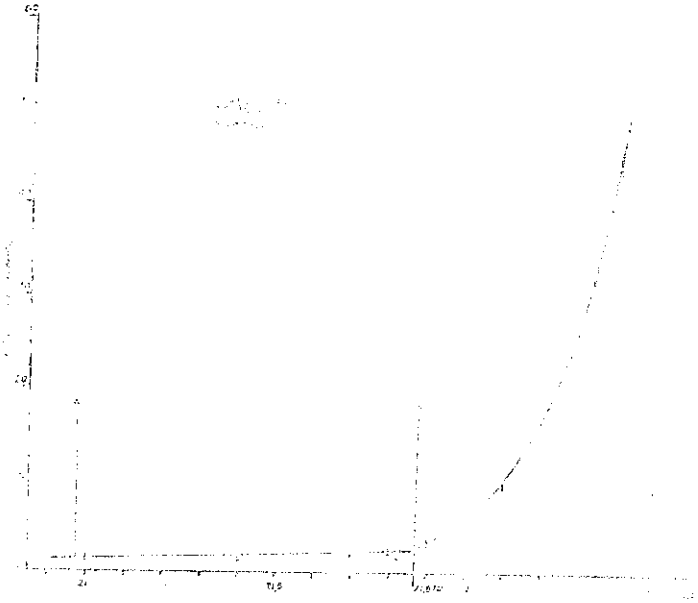

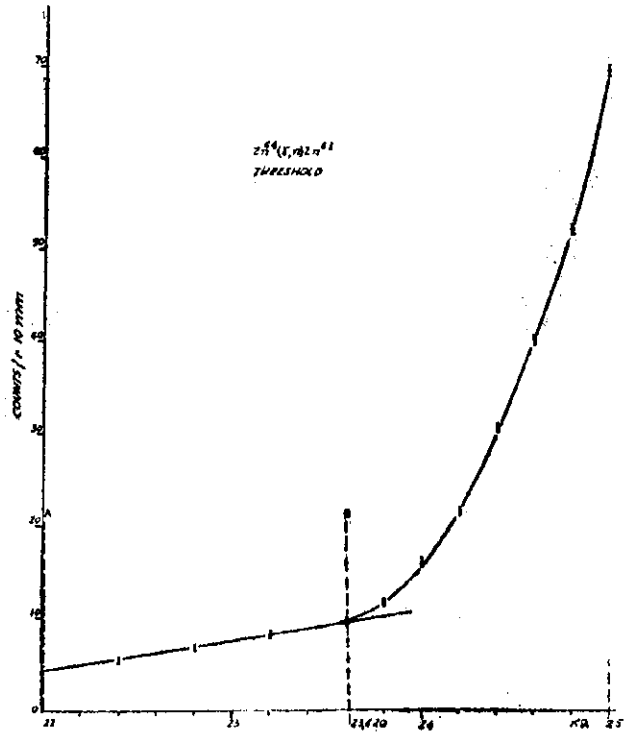

FIG. 13

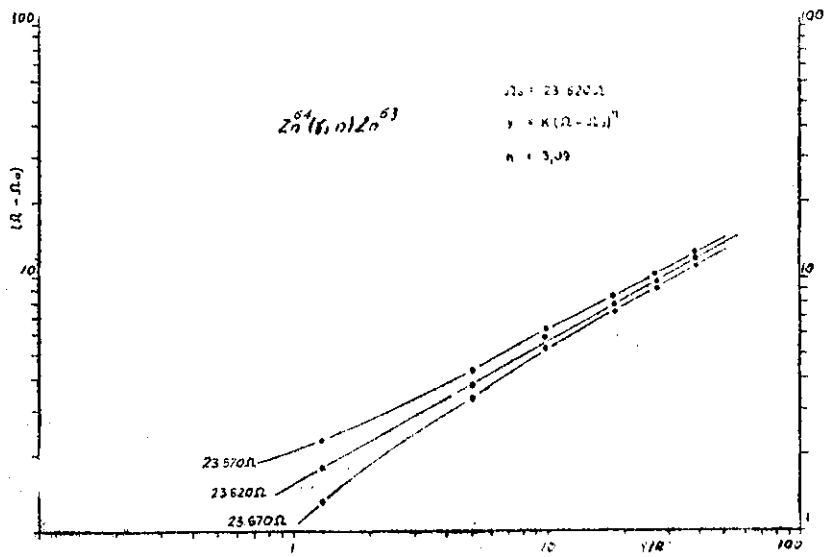

FIG. 14

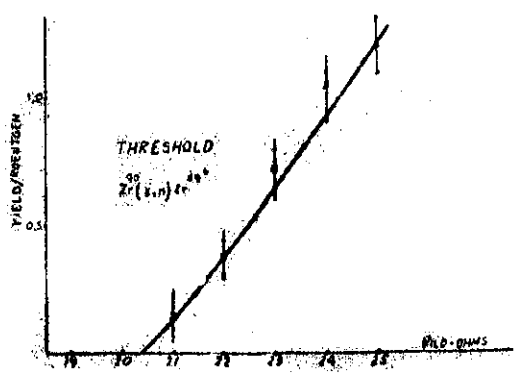

FIG 15

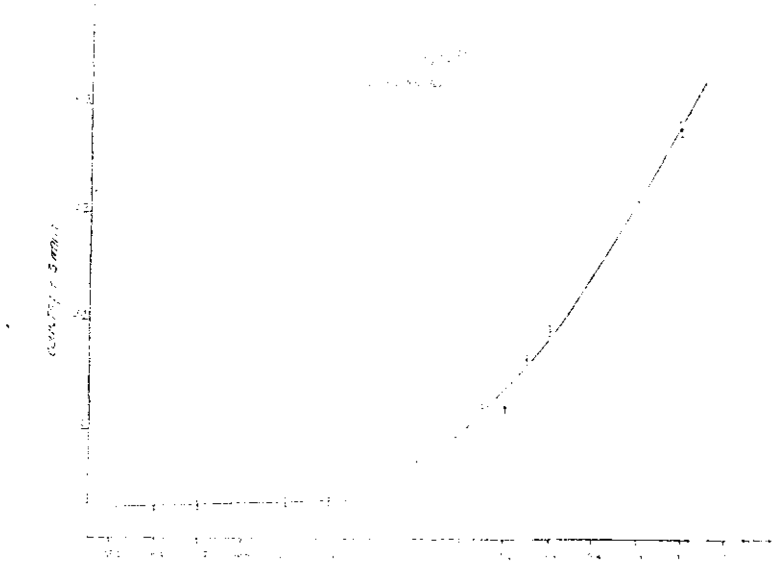

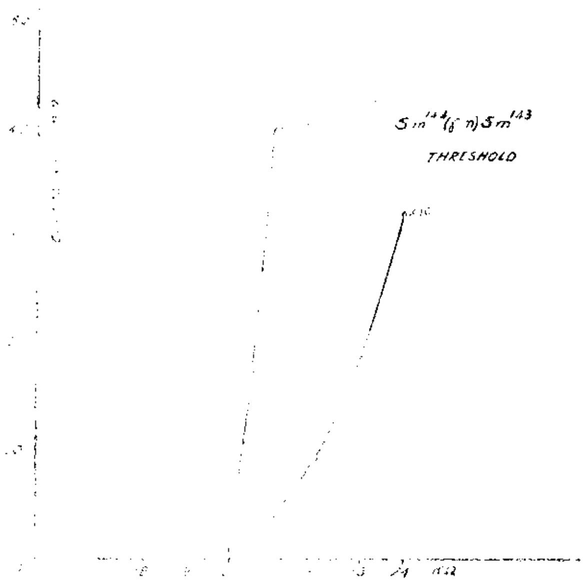

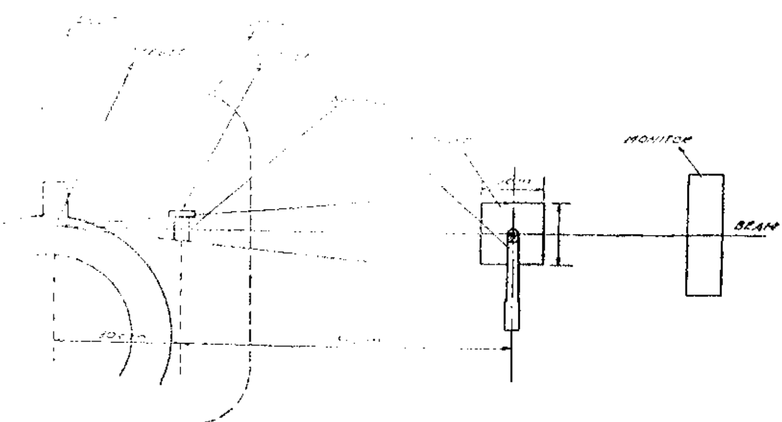

EXPERIMENTAL ... MENT

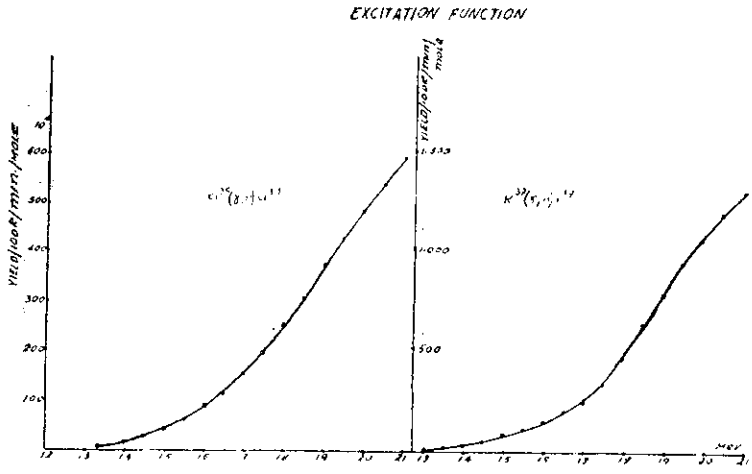

FIG. 19

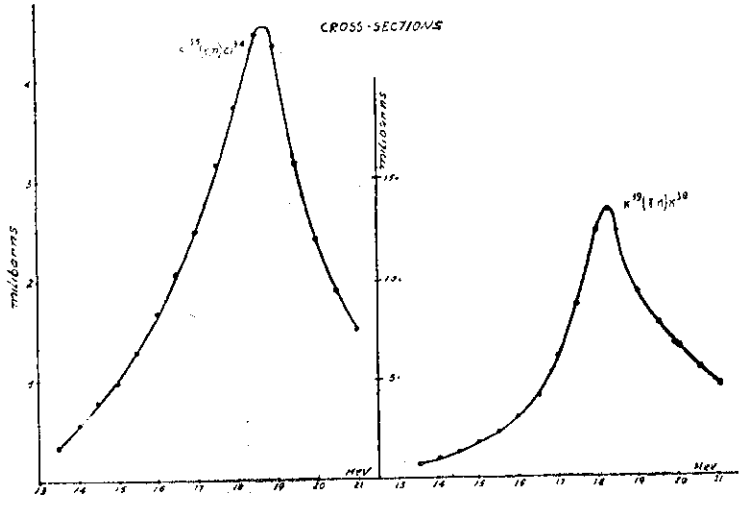

FIG. 20

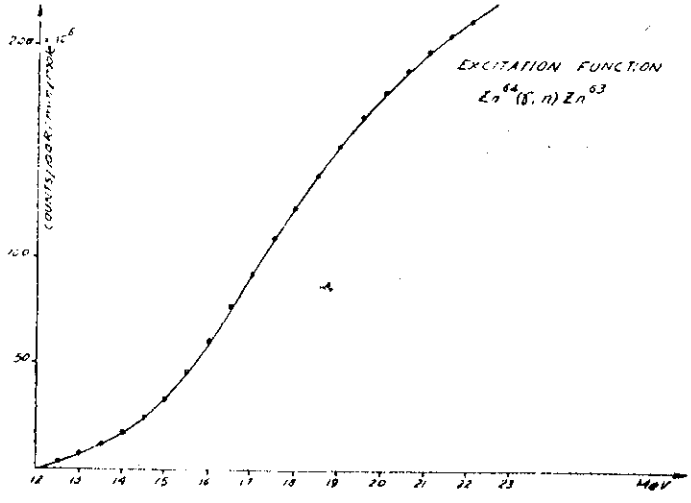

Fig. 21

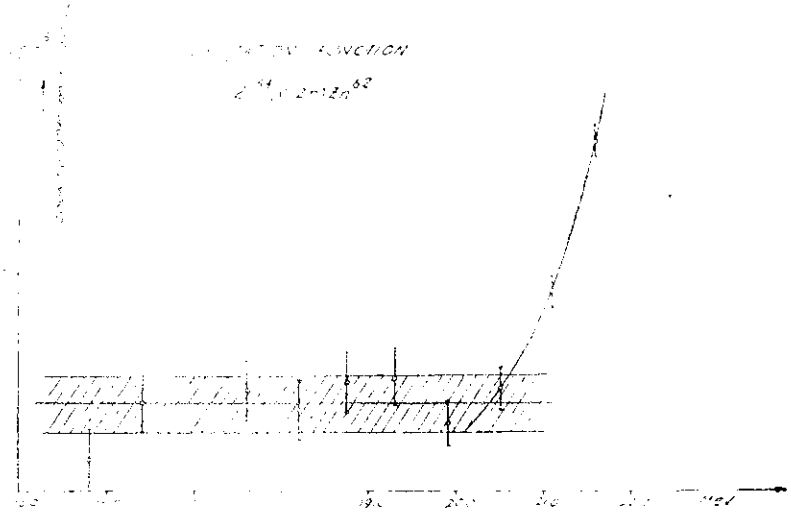

FIG. 22

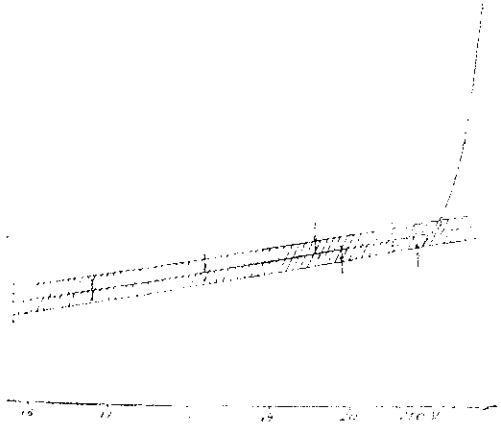

FIG. 23

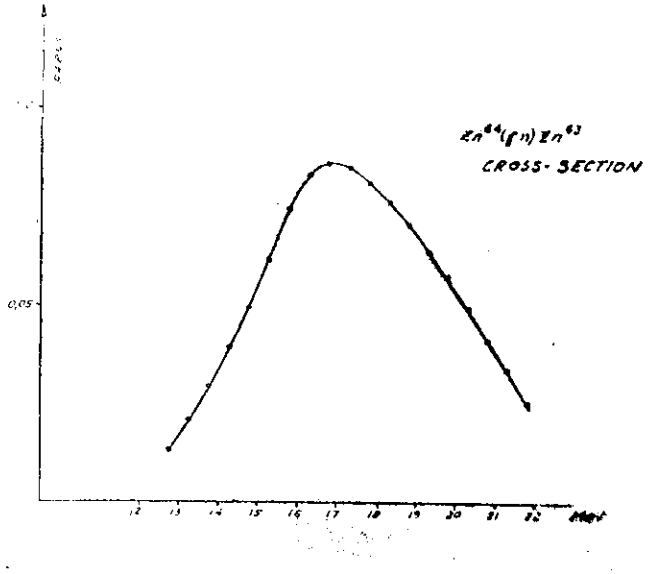

FIG. 24

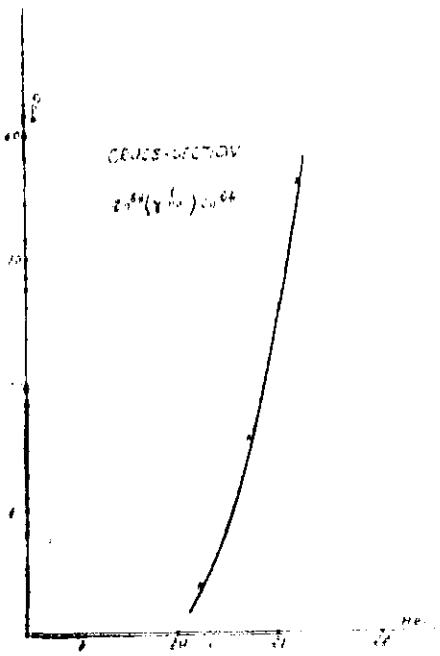

FIG 25

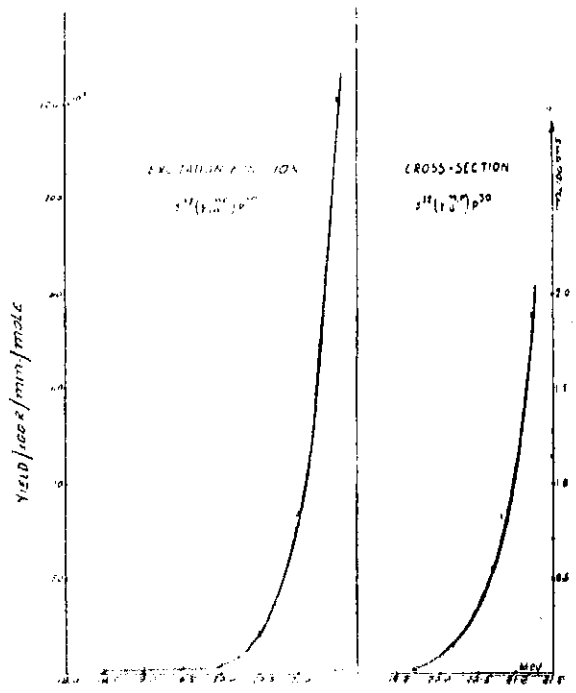

FIG

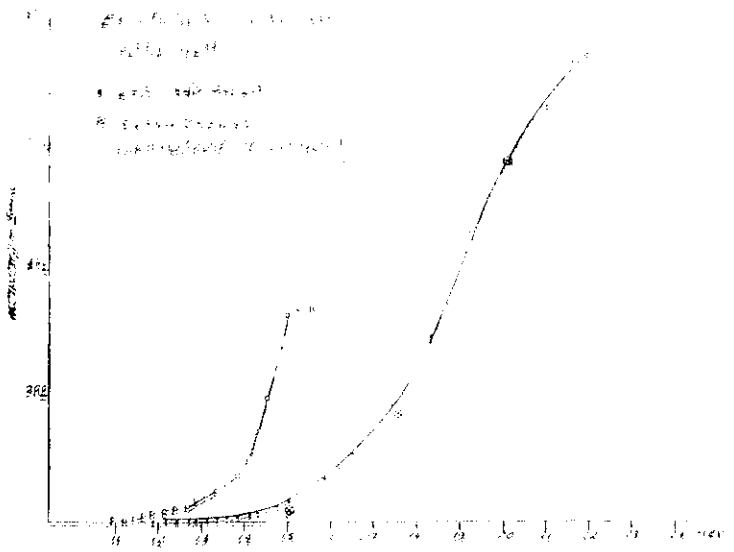

FIG 27

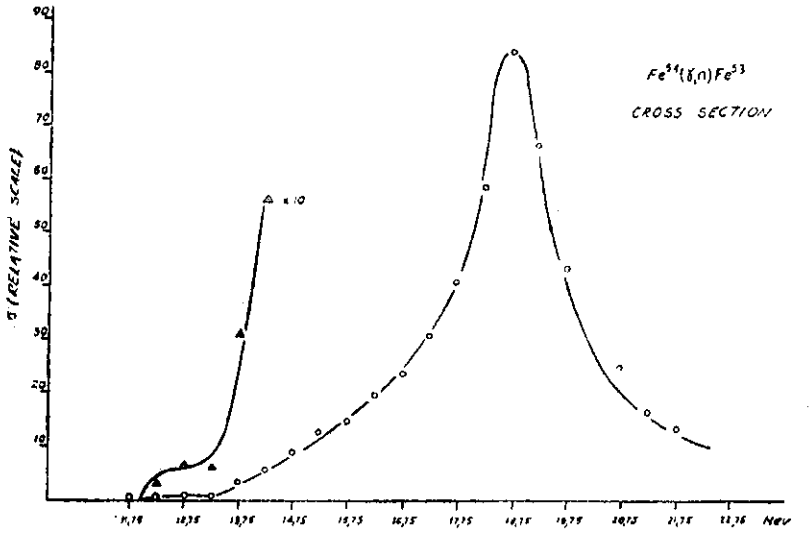

FIG. 28

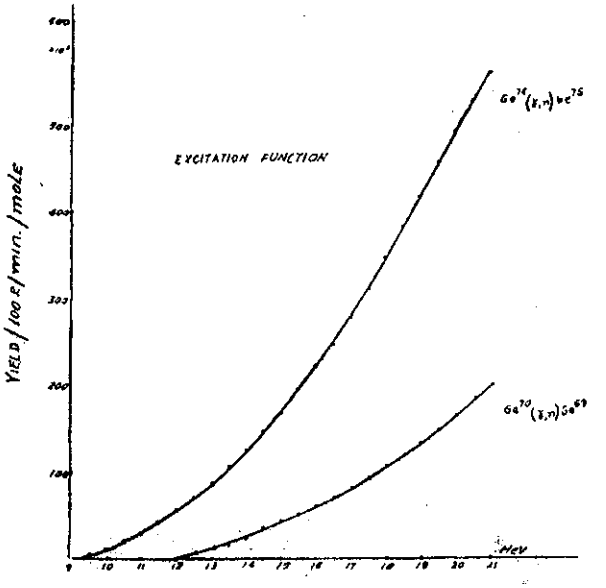

FIG. 29

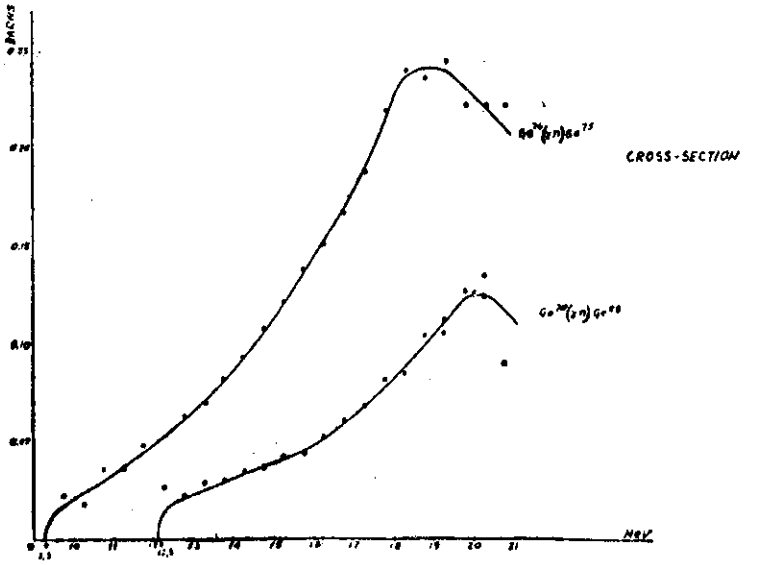

FIG. 30

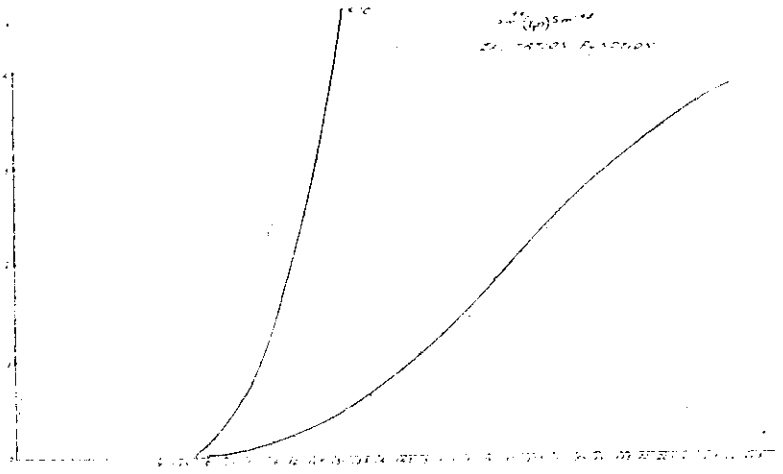

FIG 34

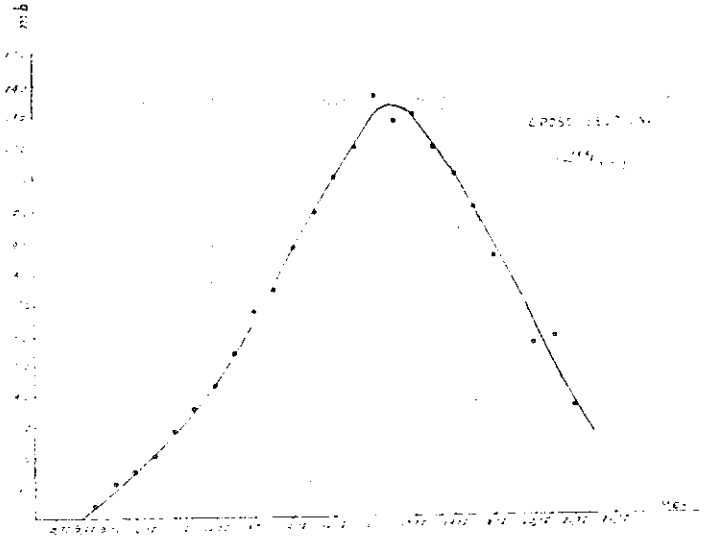

FIG 35

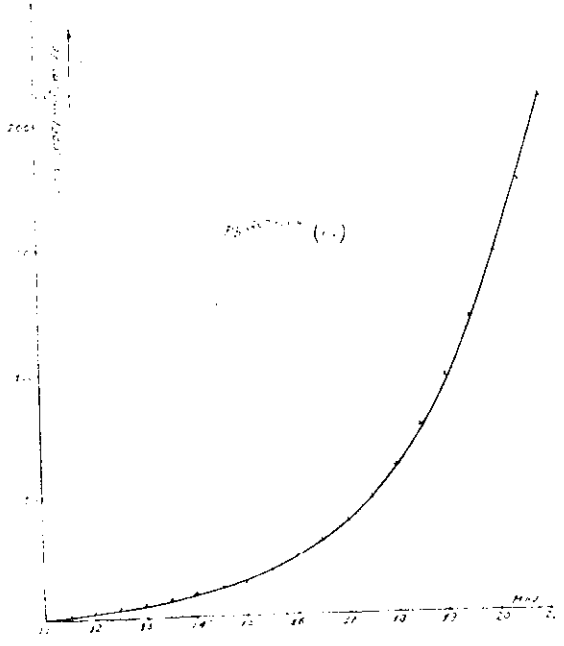

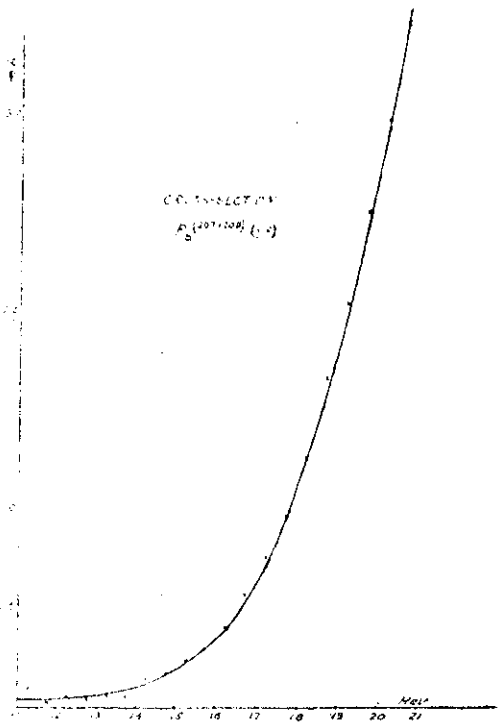

Fig. 34

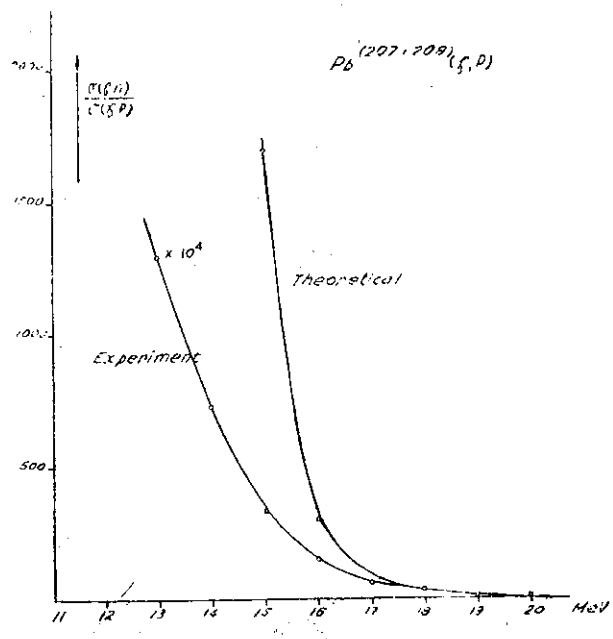

Fig. 35

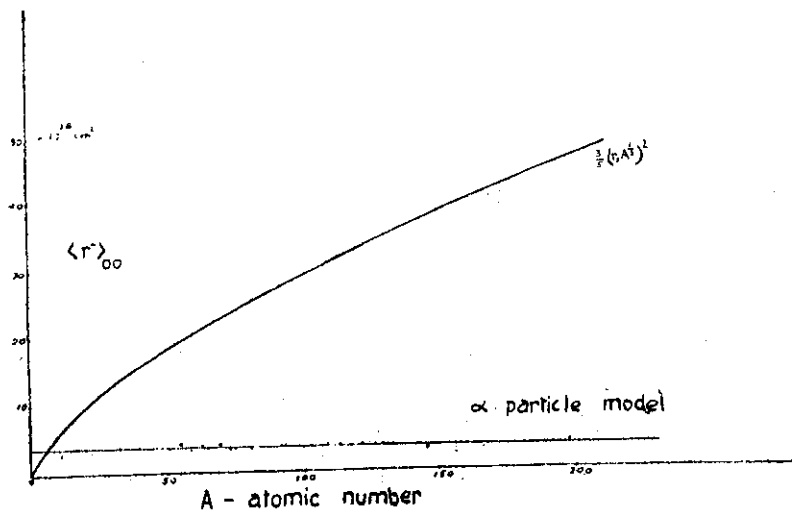

Fig. 36

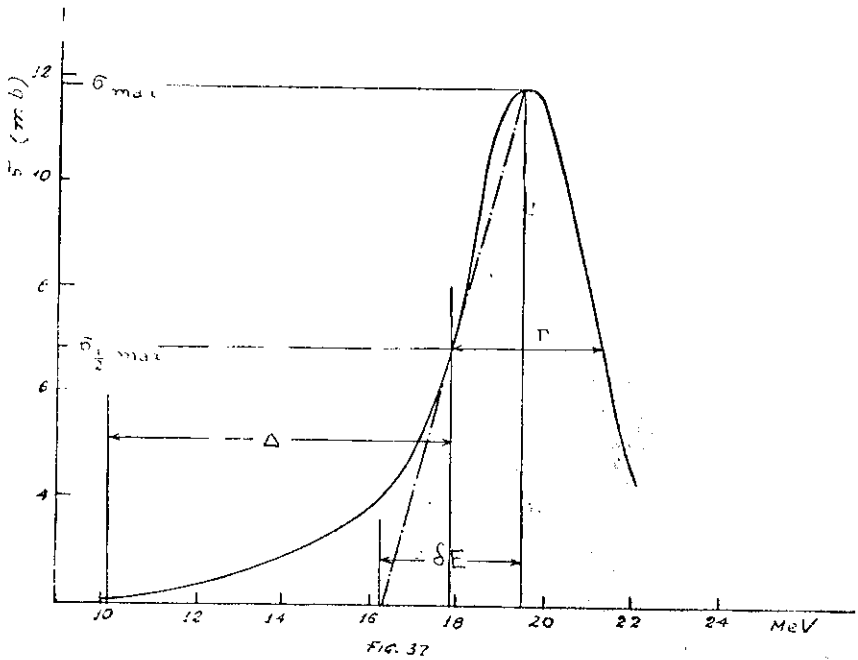

FIG. 37

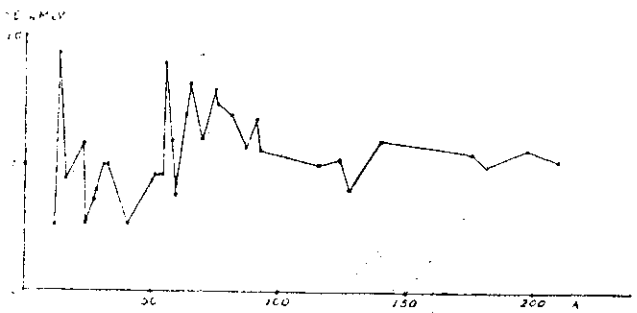

FIG. 38

SHELL EFFECT IN PHOTONUCLEAR REACTIONS

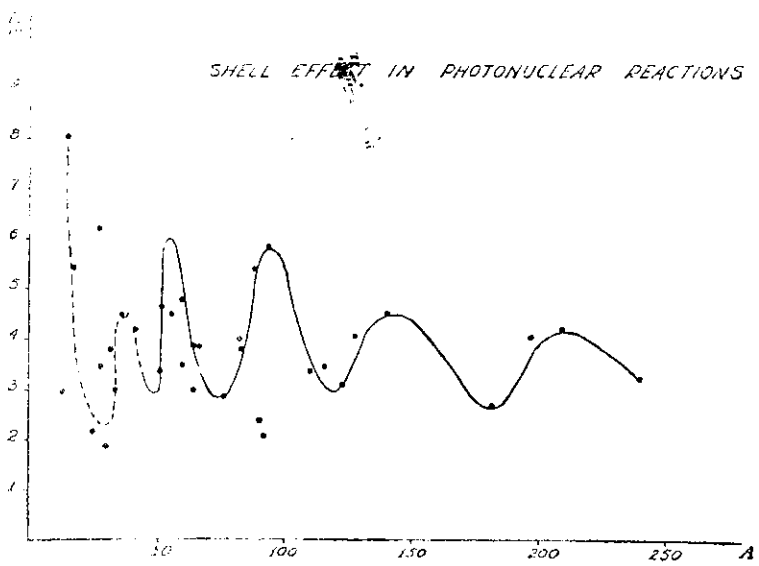

FIG. 39

12. THE FIRST EXCITED STATES OF THE C^{13}-N^{13} MIRROR PAIR ..... J. P. Davidson and J. J. Giambiagi

13. STUDIES ON THE NUCLEAR PHOTOEFFECT .. M. D. de Souza Santos, J. Goldemberg, R. R. Pieroni, E. Silva, Ottavia A. Borrello, Suzanna S. Villaça and J. Leite Lopes

I N D I C E

N O T A S D E F Í S I C A

V O L U M E I I

(1954-1955-1956)

1. THE RING FOCUS IN THE SPIRAL ORBIT SPECTROMETER... L. Marques

2. THE PHOTONUCLEAR EFFECT AND COMPLEX POTENTIAL-WELL NUCLEAR MODEL ..... J. P. Davidson

3. RANGE OF 208 ± 4 MEV PROTONS IN G5 NUCLEAR EMULSION .... Hervásio G. de Carvalho and Jerome I. Friedman

4. SHELL EFFECT ON PHOTONUCLEAR REACTIONS ..... J. Goldemberg and J. Leite Lopes

5. NOTE ON THE NON RELATIVISTIC EQUATION FOR SPIN 1/2 AND 1 PARTICLES WITH ANOMALOUS MAGNETIC MOMENT .... J. J. Giambiagi

6. RELATIVISTIC THEORY OF SPINNING POINT PARTICLES ... J. Tiomno

7. THE FORMATION OF P^{32} FROM ATMOSPHERIC ARGON BY COSMIC RAYS ..... L. Marques and Neyla L. Costa

8. EFFECT OF THE FINITE SIZE OF THE NUCLEUS ON μ-PAIR PRODUCTION BY GAMMA RAYS ..... George H. Rawitscher

9. POLARIZATION OF SPIN ONE PARTICLES ..... Samuel W. Mac-Dowell

10. EAST-WEST ASYMMETRY OF POSITIVE AND NEGATIVE MESONS AT THE GEOMAGNETIC EQUATOR ... I. Escobar V. and F. D. Harris

11. RADIATION FIELD OF AN OSCILLATING DIPOLE - I ..E. M. Ferreira